Matter

Article

Thermoelectric-flow synergy for femtosecond laser writing of iced ferroelectric nematics

Graphical abstract

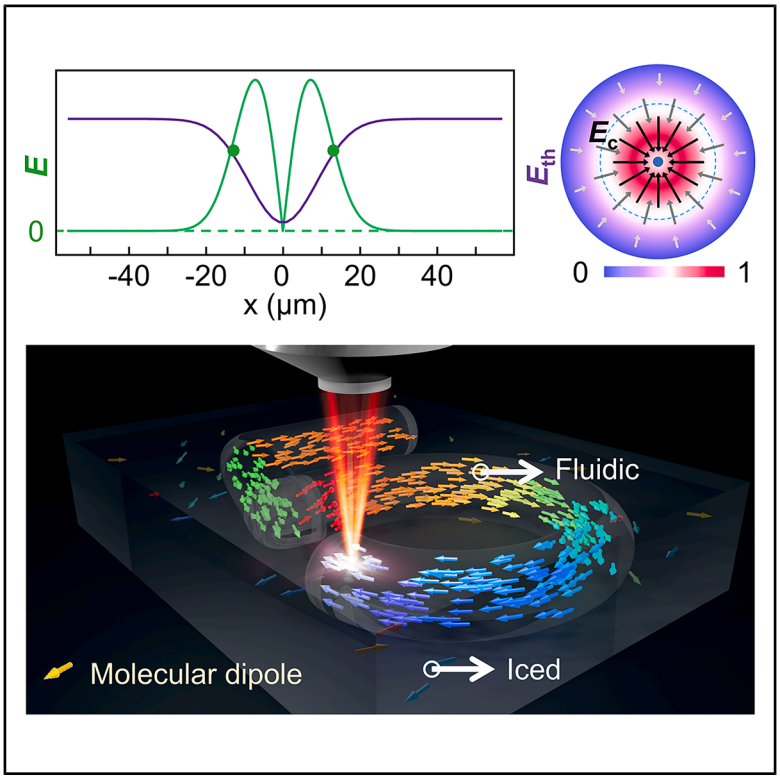

Highlights

- Unveiling thermoelectric-flow synergistic laser writing mechanism
- All-optical ferroelectric domain patterning in iced ferroelectric nematics
- Direct writing of polar liquid crystal-based nonlinear optical devices

Authors

Chao Chen, Xiao-Yi Xu, Ke-Yi Guo, ..., Lu Han, Yong Zhang, Yan-Qing Lu

Correspondence

malingling@nju.edu.cn (L.-L.M.), zhangyong@nju.edu.cn (Y.Z.), yqlu@nju.edu.cn (Y.-Q.L.)

In brief

While the emerging ferroelectric fluids hold promise for advanced photonics, patterning their room-temperature "iced" state has remained a major challenge. Here, the authors demonstrate that femtosecond laser direct writing can precisely engineer polar domains by exploiting a synergy of thermoelectric and flow effects. This approach transforms the previously unpatternable material into a versatile platform for complex nonlinear optical devices. Their work establishes a robust strategy for programming nonlinear photonic metamaterials.

1 Discovery
A new material or phenomena

Chen et al., 2026, Matter 9, 102766
July 1, 2026
https://doi.org/10.1016/j.matt.2026.102766

CellPress

Please cite this article in press as: Chen et al., Thermoelectric-flow synergy for femtosecond laser writing of iced ferroelectric nematics, Matter (2026), https://doi.org/10.1016/j.matt.2026.102766

Matter

CellPress

Article

Thermoelectric-flow synergy for femtosecond laser writing of iced ferroelectric nematics

Chao Chen,[1,2,3,4,6] Xiao-Yi Xu,[1,2,3,4,6] Ke-Yi Guo,[1,2,3,4,6] Zhao-Xian Chen,[1,2,3,4,6] Jin-Tao Pan,[1,2,3,4,6] Ling-Ling Ma,[1,2,3,4,8,*] Bo-Han Zhu,[1,2,3,5,4] Min-Xing Xu,[1,2,3,4] Yang Wei,[1,2,3,4] Chen-Zhu Xie,[1,2,3,4] Lu Han,[1,2,3,4] Yong Zhang,[1,2,3,4,*] and Yan-Qing Lu[1,2,3,4,7,*]

[1]National Laboratory of Solid State Microstructures, Nanjing University, Nanjing, China
[2]Key Laboratory of Intelligent Optical Sensing and Manipulation, Nanjing University, Nanjing, China
[3]Collaborative Innovation Center of Advanced Microstructures, Nanjing University, Nanjing, China
[4]College of Engineering and Applied Sciences, Nanjing University, Nanjing, China
[5]School of Electronis Science and Engineering, Nanjing University, Nanjing, China
[6]These authors contributed equally
[7]Senior author
[8]Lead contact
*Correspondence: malingling@nju.edu.cn (L.-L.M.), zhangyong@nju.edu.cn (Y.Z.), yqlu@nju.edu.cn (Y.-Q.L.)
https://doi.org/10.1016/j.matt.2026.102766

PROGRESS AND POTENTIAL Femtosecond laser direct writing has revolutionized micro-manufacturing in hard materials, yet its potential for manipulating soft, dynamic phase-transitioning systems remains largely unexplored. This work bridges this gap by introducing a method to directly write ferroelectric domains in "iced" ferroelectric nematic liquid crystals—a promising material state previously considered unpatternable at room temperature due to the failure of conventional alignment techniques. By uncovering a novel mechanism where laser-induced thermoelectric fields and fluid shear flow work synergistically, we achieved precise, electrode-free control over molecular ordering without material damage.

This breakthrough transforms a disordered, solid-like material into a versatile, programmable platform for advanced nonlinear photonics. Looking forward, this technology paves the way for the development of reconfigurable iced nonlinear optical devices that bridge fundamental soft matter physics with practical applications. The ability to locally engineer nonlinear optical properties offers immense potential for developing ultrafast all-optical switches, high-density non-volatile memory, and programmable quantum light sources for entangled photon generation. Furthermore, this platform could enable complex structured light generation, such as optical skyrmions, accelerating advancements in next-generation optical computing and dynamic holographic imaging.

SUMMARY

Femtosecond laser writing stands as a cornerstone of modern photonics, enabling both fundamental research into light-matter interactions and manufacturing of devices with multiplexing functionalities. However, direct writing of polar ordering in complex multi-phase systems remains unexplored. We demonstrate the direct writing of ferroelectric domains in an iced ferroelectric nematic liquid crystal where conventional alignment fails. We reveal that the writing mechanism is a phase-transition cooperative assembly process, where laser-induced shear flow and localized thermoelectric fields collaboratively dictate the final polar architecture. This mechanism enables precise engineering of diverse domain patterns, ranging from single-line to radially arrayed structures. As proof of concept, we showcase laser-written nonlinear Raman-Nath gratings that enable efficient frequency doubling and beam steering and further advance the generation of second-harmonic optical vortices carrying orbital angular momentum. Our work establishes a versatile platform for domain engineering in soft ferroelectric matter, opening new routes toward on-demand nonlinear photonic metamaterials.

Please cite this article in press as: Chen et al., Thermoelectric-flow synergy for femtosecond laser writing of iced ferroelectric nematics, Matter (2026), https://doi.org/10.1016/j.matt.2026.102766

INTRODUCTION

Femtosecond laser direct writing has revolutionized the fabrication of photonic devices and functional microstructures in materials ranging from glasses to crystals.[1–5] Its unique capability for three-dimensional processing[6] enables the creation of embedded waveguides,[7] optical memories,[8] and nonlinear components with exceptional precision. The interaction of an ultrafast laser pulse with a material usually induces highly nonlinear absorption, leading to localized and permanent modifications of material properties.[9] This versatility has established femtosecond laser writing as an indispensable tool in integrated photonics and quantum optical technology.[10] However, the vast majority of these applications exploit modifications in the solid state, where the material response is essentially static and governed by defect generation or ablation. The exploration of this powerful technique in dynamic, soft systems, particularly those exhibiting complex phase transitions and fluidity, remains a significant frontier.

The recent discovery of ferroelectric nematic liquid crystals (FNLCs),[11–17] such as RM734,[11] presents a tantalizing arena for laser writing. These materials combine the fluidity and self-assembly of LCs with robust spontaneous polarization,[14,18–23] offering immense potential for electro-optics and nonlinear photonics.[13–16,18–20,24,25] Such phase typically exists at elevated temperatures, and at room temperature, the ferroelectric nematic materials are in a disordered polycrystalline state. A grand challenge, however, lies in the deterministic domain engineering of these materials—especially in their crystalline-like "iced" state—to easily harness their nonlinear properties. Conventional alignment techniques prove ineffective for patterning this particular phase, creating a critical fabrication bottleneck. Although direct laser writing of LCs has been explored,[26–29] previous strategies primarily relied on modifying surface alignment layers and two-photon polymerization. In contrast, the laser-matter interaction in the bulk iced ferroelectric phase involves direct coupling with the LC medium, governed by complex hydrodynamic and thermal dynamics. The fundamental physics of how an ultrafast laser interacts with such a multi-phase system—navigating through fluid, polar, and solid-like states—to define a spontaneous polar order is virtually unknown.

Here, we bridge this critical gap by introducing a versatile femtosecond laser direct-writing technique for reconfigurable domain engineering in iced FNLCs at room temperature. We systematically investigate the anisotropic linear and nonlinear optical properties of the iced RM734 material and develop a low-power-density writing strategy that leverages nonlinear absorption to locally modify the spontaneous polarization without material damage. A systematical investigation of laser parameter dependence reveals rich underlying physics: especially at elevated powers, domain formation is governed by a unique multi-phase cooperative self-assembly process, where laser-induced thermoelectric fields and shear flow-induced alignment act in concert to define the polar ordering. The resulting domain structures exhibit distinct morphologies, including line domains with embedded substructures, characterized by a polarized optical microscope (POM) and corroborated by theoretical modeling. As proof of concept, we demonstrate the direct writing of complex $\chi^{(2)}$ patterns for advanced nonlinear wavefront shaping, including nonlinear diffraction gratings for nonlinear beam steering and a fork grating for generating second-harmonic optical vortices. These results highlight the versatility of our approach in programming adaptive and reconfigurable nonlinear photonic devices, bridging fundamental studies in soft condensed matter physics with practical applications in integrated optics and quantum optics.

RESULTS

Optical properties

RM734[11,30–32] (Figure 1A), representing a paradigmatic ferroelectric nematic system, is favored due to its stability, high dielectric constant (ε), and larger second-harmonic nonlinear coefficient ($\chi^{(2)}$) in its ferroelectric nematic phase.[18] Its phase transition process is provided in Figures S1A and S1B, utilizing a combination of POM and differential scanning calorimetry. The compound demonstrates an isotropic-to-nematic phase transition at $T_{I\text{-}N}$ = 183°C (I, isotropic phase; N, nematic phase), a nematic-to-second-nematic transition at $T_{N\text{-}NF}$ = 127.8°C (NF, ferroelectric nematic phase), and an indeterminate crystallization point generally occurring below 70°C during the cooling process. After the RM734 is infiltrated into an unidirectionally aligned cell, a frosted granular POM texture with iced disordered LC domains (Figure S1C) develops from a twisted ferroelectric nematic structure when the material is cooled to room temperature (25°C). The transmittance spectrum (Figure S2) confirms that the optical band gap E_g of the iced RM734 exceeds the energy of two photons (3.10 eV) but is less than that of three photons (4.65 eV) at the 800 nm excitation. This condition ($2\hbar\omega < E_g < 3\hbar\omega$) facilitates a resonant-enhanced three-photon absorption process,[33] enabling efficient energy deposition into the transparent film to trigger the localized temperature change required for writing. Detailed materials, fabrications, and characterizations of iced ferroelectric nematic samples are provided in methods.

The optically anisotropic property of photoaligned iced ferroelectric nematics is characterized using a POM, showing no extinction of the iced FNLC film when rotating the cell. The extracted brightness of these textures indicates a continuous variation, with a ~10.0% difference between the maximum and minimum (Figure S1D). Moreover, the second-order nonlinear optical response and its polarization dependency of the unidirectionally aligned iced RM734 further confirm its weak optical anisotropic property of the iced RM734 (Figure S3). Thus, such iced ferroelectric nematics is fundamentally different from the ordinary high-temperature ferroelectric nematic phase, constituting a unique family of nonlinear optical materials. Despite its potential in materializing diverse polar optical structures, photoalignment fails to pattern the iced ferroelectric nematic phase of RM734 (see Figures S1E–S1G; Note S1).

Femtosecond laser writing of iced ferroelectric nematics

Femtosecond laser writing has emerged as a powerful and versatile technique in micro- and nano-manufacturing, offering exceptional precision in fabricating complex structures across diverse materials.[34–37] Here, we adopt femtosecond laser

Please cite this article in press as: Chen et al., Thermoelectric-flow synergy for femtosecond laser writing of iced ferroelectric nematics, Matter (2026), https://doi.org/10.1016/j.matt.2026.102766

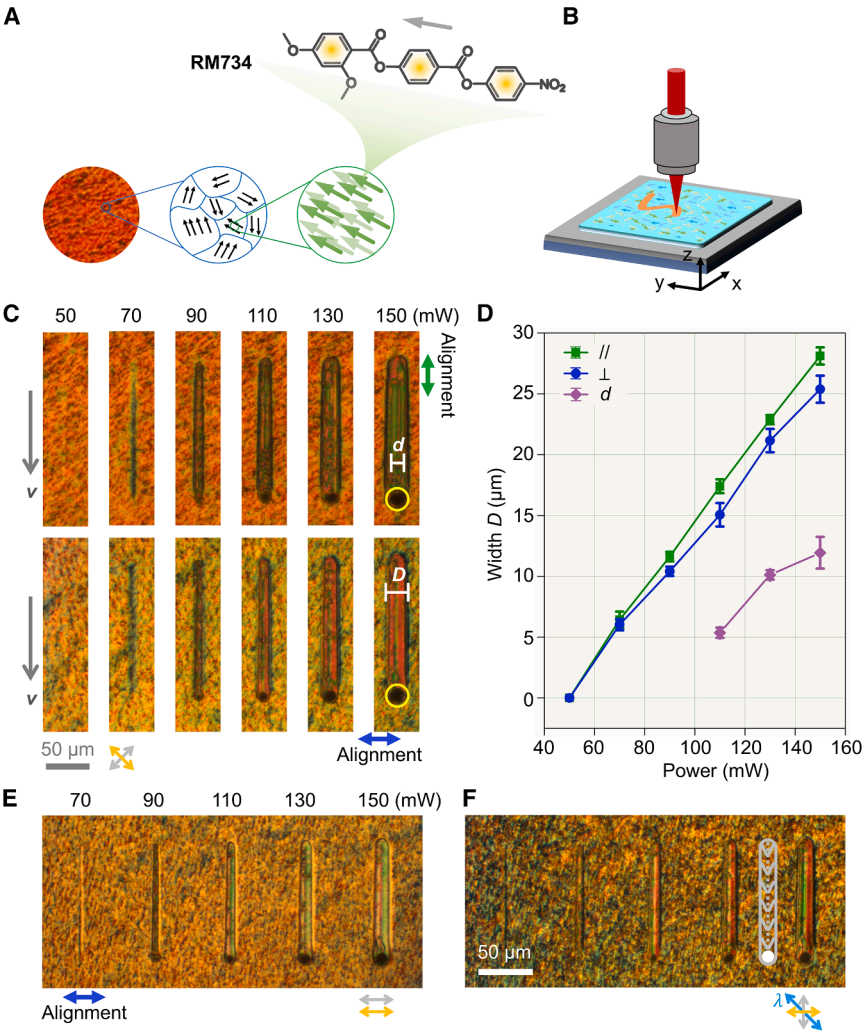

Figure 1. Femtosecond laser writing of iced RM734 material

(A) Schematics of the ferroelectric domains in iced RM734 and the chemical structure of RM734.

(B) Schematics of femtosecond laser writing of iced RM734 domains.

(C) Line domains written by a femtosecond laser with varied pulse energies (ranging from 50 to 150 mW at an interval of 20 mW) and different laser scanning directions (parallel and perpendicular to the alignment direction). The double-edged green and blue arrows denote the photoalignment direction of the LC cell. The transmission axes of the polarizer and analyzer are indicated by gray and yellow arrows, respectively. The scale bars are 50 μm.

(D) Relationship between the line domain width *D*, embedded domain width *d* (in purple), and the femtosecond laser power. The green line illustrates the variation in domain width when the laser writing direction is parallel to the alignment, whereas the blue line represents the condition when it is perpendicular.

(E and F) Line domains observed under different conditions. The used femtosecond laser power ranges from 70 to 150 mW at an interval of 20 mW. The double-edged blue arrows denote the photoalignment direction of the LC cell. The double-edged sky-blue arrows denote the slow axis of the full-wave plate. The transmission axes of the polarizer and analyzer are indicated by gray and yellow arrows, respectively. The scale bars are 50 μm. The inset shows a schematic of the LC director after direct writing.

direct writing to achieve an effective polar ordering control in the room-temperature RM734 material. Our experimental setup for the femtosecond laser direct writing of iced ferroelectric nematic materials is illustrated in Figures 1B and S4. Figures 1C and S5 demonstrate two scenarios of laser writing of iced RM734 at different pulse powers. The iced RM734 material (film thickness ~10 μm) is unidirectionally photoaligned. The laser beam is focused using a 10× objective (*NA* = 0.3). The theoretical diffraction-limited spot size is approximately 5 μm in diameter based on the effective numerical aperture ($NA_{eff} \approx 0.196$, calculations in Note S2). However, it should be noted that the effective writing resolution is governed by the combination of thermal field distribution and the threshold of polar LC switching. The scanning velocity is kept constant at 10 μm/s, and the writing direction is either along or perpendicular to the preset alignment direction. Below the threshold power (50 mW), no change in texture is observed. With the gradual increase in pulse power, the laser-written traces become increasingly distinct, signifying tunable degrees of modification in the iced ferroelectric domains. When the power exceeds 90 mW (90–150 mW), thicker domains are imprinted into the RM734 film, exhibiting clearly defined dark boundaries. For samples using rubbed polyimide alignment layers, significantly higher laser powers (370–520 mW) are required to initiate domain writing (Figure S6). This power disparity arises from the anchoring energy difference: rubbed polyimide provides strong anchoring (~10^{-4} J/m^2),[38] necessitating a stronger driving force to overcome surface pinning compared to the weak anchoring of photoalignment (~10^{-6} J/m^2).[39] Therefore, compared to samples with photoalignment (Figure S1C and 1D), rubbing-aligned samples exhibit stronger bright-dark contrast (Figure S7). Notably, laser-induced fluidity is observed during the writing process when the laser power exceeds 90 mW (Video S1). In these domains, distinct internal morphologies are formed, characterized by embedded strip-like substructures. For the peripheral areas surrounding inner domains, optical anisotropy characterization (Figure S8) reveals a herringbone-like polar ordering. When corroborated by bright-field POM observation and retardation-plate measurements (Figures 1E, 1F, and S9), we provide clearer characterization of the alignment quality by highlighting the laser-induced polar ordering. This observation also helps us infer the LC director orientation after laser writing, as schematically illustrated in Figure 1F (more details can be found in Note S3).

Please cite this article in press as: Chen et al., Thermoelectric-flow synergy for femtosecond laser writing of iced ferroelectric nematics, Matter (2026), https://doi.org/10.1016/j.matt.2026.102766

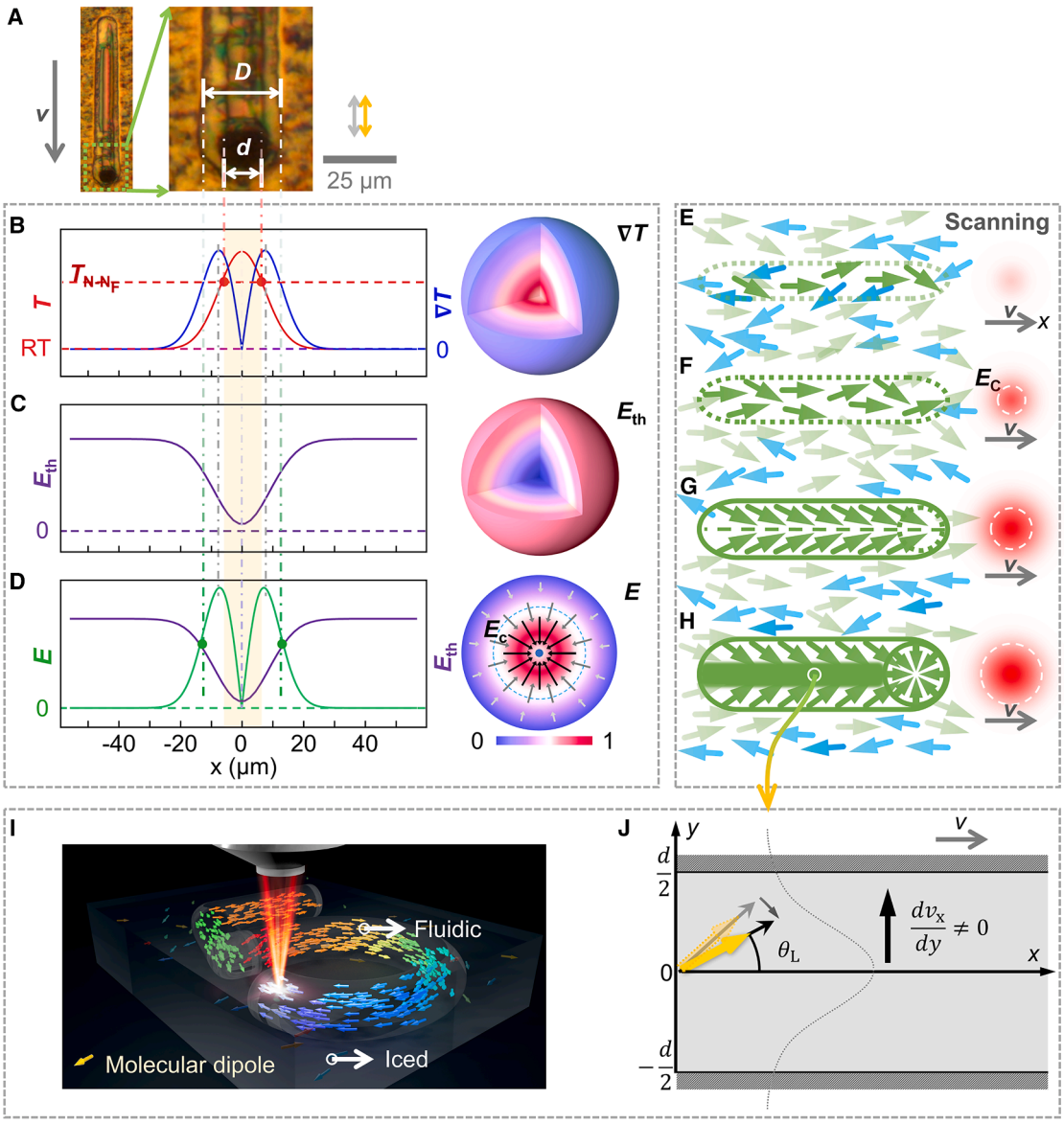

Figure 2. Working principle of the femtosecond laser writing technology for iced RM734 ferroelectric domain engineering

(A) POM texture and a magnified view of a typical line domain written with a laser power of 150 mW in photoaligned LC cells. The scale bars are 25 μm. The transmission axes of the polarizer and analyzer are indicated by gray and yellow arrows, respectively.

(B) 3D spatial gradient distribution (right) and corresponding temperature (left, red curve, RT = 20°C) and its gradient profiles (right, blue curve) along the central axis of the Gaussian spot during femtosecond laser writing.

(C) 3D distribution of the threshold electric field required for ferroelectric domain switching (right) and the corresponding threshold voltage profile along the central axis of the laser spot (left, purple curve) for iced RM734.

(D) 2D distribution of the thermoelectric field induced by the femtosecond laser (right) and the corresponding thermoelectric-field profile extracted along the central axis (left, green curve).

(E–H) Schematics of laser-written iced RM734 domains. The outcome of femtosecond laser writing in iced RM734 is strongly governed by the interplay of pulse energy (in conjunction with repetition rate) and the scanning trajectory. Green and blue arrows represent the molecular dipoles of RM734. As the laser writing direction is along the *x* axis, the thermoelectric field in the right hemisphere initially induces a specific local polarization within the iced RM734 domain. Subsequently, when the left hemisphere reaches this position, the field in the left hemisphere modifies the established polar domain, thereby determining the final domain structure. Conversely, when the laser writing direction is oriented along the negative *x* axis, the thermoelectric field in the right hemisphere assumes a decisive role in shaping the domain structure.

(legend continued on next page)

Please cite this article in press as: Chen et al., Thermoelectric-flow synergy for femtosecond laser writing of iced ferroelectric nematics, Matter (2026), https://doi.org/10.1016/j.matt.2026.102766

Quantitative analysis of the written domain lines (Figure S10) shows that while domains fabricated at lower laser powers exhibit granular textures, those undergoing a laser-induced melt-recrystallization process in the central region display higher homogeneity. As quantified in Figure 1D, both the inner width d and the outer width D of the laser-written domains exhibit a monotonic increase as the laser power rises from 110 to 150 mW. Furthermore, the domains are slightly wider in D when the writing direction is parallel to the LC alignment, compared to when the direction is perpendicular. The difference in domain widths between these two writing directions increases with laser power, reaching a maximum of approximately 10.5%, which is attributed to the nearly isotropic nature of the iced RM734 film (Figure S1D).

A distinct dark spot appears at the termination point of the laser scanning trajectory, as denoted by the yellow circle in Figure 1C, indicating the end of the line domain. We investigate whether the dark terminal spot indicates damage caused by the high-power femtosecond laser. Figure S11 illustrates elongated domains created using three different scanning pathways: unidirectional from left to right, unidirectional from right to left, and a pathway involving scanning from left to right, turning off the femtosecond laser at the right end and then resuming scanning in the reverse direction. The results show that the dark terminal spot consistently appears only once at the laser's final scanning end in all cases. This suggests that the reverse scanning process erases the previous terminal spot, indicating that the dark spots are not caused by damage.

To explain the domain formation, we propose a model combining thermoelectric fields and shear flow (Figure 2). Femtosecond laser writing typically exploits the nonlinear absorption of femtosecond pulses by the material to generate thermal energy, with thermal accumulation driven by high repetition rates. This results in elevated temperatures and steep temperature gradients within the focal volume of the optical beam.[40] Our quasi-steady-state thermal simulations (Note S4; Figures 2B, S2, and S12) reveal an extremely steep temperature gradient ($\nabla T = 10^7$ K/m) localized within the material. Although organic materials typically possess a low Seebeck coefficient, this steep temperature gradient generates a substantial bulk thermoelectric field $\boldsymbol{E} = S_{ij}\nabla T \approx 10^5$ V/m (Figure S12C). Simultaneously, the temperature rise reduces the coercive field (E_{th}) of the material (Figures 2C and S12D, measurements in S12E, and S12F). Domain switching occurs selectively in the annular region where the induced thermoelectric field exceeds the local coercive field ($E > E_{th}$, Figure 2D). The laser scanning velocity plays a pivotal role in defining the domain quality. Our investigation reveals that increasing the writing speed reduces the time for re-orientation or/and crystal growth, which leads to a reduction in domain uniformity (Figures S13 and S14). Consequently, an intrinsic trade-off exists between fabrication throughput and structural homogeneity, necessitating a careful optimization of the writing speed (typically maintained at 10 μm/s in this work) to ensure robust polar ordering.

Concomitantly, at higher laser powers, the central region undergoes a transient phase transition into the fluid state. The localized solid-to-liquid transition, combined with the spatial translation of the laser beam, induces a material flow that overcomes the initial surface anchoring, resulting in shear-flow alignment. It was established in the 1980s that shear flows of sufficient strength in low-molar-mass[41] and polymeric nematic LCs[42] can induce significant textural changes accompanied by disclinations, a behavior later analyzed theoretically.[43,44] In our system, the laser-induced melting and laser scanning processes lead to flow, operating at a high Ericksen number. This hydrodynamic dominance may force the melted LC director to deviate from the preset surface anchoring and enter a flow-aligned regime. Specifically, a viscous torque acts on the rod-like RM734 molecules, driving their reorientation against random thermal motion. This torque originates from the differential hydrodynamic resistance—defined by the velocity gradient ($\frac{\partial v_x}{\partial v_y} \neq 0$, Figures 2I and 2J)—experienced by the anisotropic molecules, which causes the director n to rotate toward a stable equilibrium orientation known as the Leslie angle (θ_L). In most nematic systems, this orientation lies nearly parallel to the flow direction, corresponding to a state of minimal energy dissipation.[3,45] Thus, under laser-directed shearing, the molecular alignment is dictated by the balance between viscous torques and rotational diffusion, leading to a macroscopically ordered state. In rare instances, flow-induced disclination loops are also observed (Figure S15), which may be attributed to the backflow effect, i.e., flow reversal. When the flow ceases or changes abruptly, the release of stored elastic energy causes the director to rotate continuously within the shear plane.[44]

We schematically summarize the laser writing process and the resultant domain structures in Figures 2E–2H. Once the electric field exceeds the threshold (experimentally, 50 mW for a photoaligned sample, and the results for rubbing-aligned samples are shown in Note S5 and Figure S6), it induces varying degrees of modification of the iced RM734 material (Figures 2E and 2F). When the thermoelectric field significantly surpasses the threshold without reaching the "explosion" (damage) threshold, the spontaneous polarization of iced RM734 tends to reorient according to the local thermoelectric field (Figures 2G and 2H). In this process, the laser writing direction also plays a crucial role, which determines the final interaction between the electric field and RM734 for domain engineering (see figure caption). In addition, a phase transition and flow effect[3] are induced in the central region of the focal spot. Following laser writing, the RM734 material recrystallizes into

(I and J) Schematics of higher laser power-induced phase transition and shear-flow effect in LCs. (I) The FNLC dipoles, represented by the colored unidirectional arrows. The red beam denotes the femtosecond laser used for writing. (J) A top-view schematic of a localized region during the direct laser writing process shown in (I), with the yellow arrows indicating the orientation of the molecular dipole. The dark gray areas correspond to regions unaffected by phase transition, whereas the light gray zones indicate phase-transformed regions. Within a zone of width d, scanning of the laser spot combined with phase transition generates a fluid flow. Due to the difference in physical parameters such as interfacial tension near and away from the transition boundary, a flow field is produced, which in turn drives the reorientation of the ferroelectric nematic dipoles. The dashed gray curves schematically depict the non-uniform velocity profile of the flow. This representation is intended as a schematic illustration of the process.

Please cite this article in press as: Chen et al., Thermoelectric-flow synergy for femtosecond laser writing of iced ferroelectric nematics, Matter (2026), https://doi.org/10.1016/j.matt.2026.102766

a ferroelectric line domain featuring a central embedded defect line. The dark terminal spot in Figure 2A is a specific polar structure due to the spherically radial nature of the thermoelectric field and the large accumulation of pulse energy resulting from the delayed response of the optical shutter. This phenomenon is in alignment with the spherulites reported in Liu et al.[46] This synergic mechanism paradigm—combining thermoelectric-field-driven polarization switching in the periphery with shear-flow-directed alignment in the center—establishes a framework for laser processing of soft ferroelectric systems, enabling unprecedented control over domain architectures in ferroelectric nematics.

Nonlinear beam steering

By leveraging the laser writing technique, we are now able to rationally design and flexibly engineer the polar ordering of iced RM734 microstructures (Figures 3 and S16) to locally modify the effective nonlinear coefficient for photonic functionalities. Three types of structures—a circular configuration, a radial line domain array, and a grating—are fabricated as proof-of-concept demonstrations by directing an 800-nm laser beam to pole the rubbing-aligned (Figure 3) and photoaligned iced RM734 materials (Figure S17). As shown in Figures 3C and 3D, the domain widths exhibit periodic changes (e.g., from 3 to 9 μm for radial line domains) depending on the azimuthal angle φ. Specifically, the width of the line structure is maximum when the laser writing direction is parallel to alignment and at its minimum when it is perpendicular. The domain width difference of the rubbing-aligned sample is larger than that of the photoaligned iced RM734, which is attributed to an order-of-magnitude stronger anchoring energy provided by the unidirectionally rubbing-aligned substrates.[27,38,39] It results in a stronger optically anisotropic property, thereby affecting the laser writing behavior. More details can be found in Note S5.

Figures 3E, 3F, and S17 show the Raman-Nath diffraction patterns of different nonlinear gratings. The periodic line domains in Figure 3E are fabricated by sequentially applying the femtosecond laser "pencil" to write along the alignment direction. We found that the domains modified by the laser exhibit a stronger second-harmonic signal (Figure S18), which confirms that femtosecond laser writing can effectively modify the second-order nonlinear coefficient of the RM734. Its phase-matching condition[47] can be articulated as follows:

$$\boldsymbol{k}_{2\omega} = 2\boldsymbol{k}_{\omega} + \boldsymbol{G}_n, \qquad \text{(Equation 1)}$$

where $\boldsymbol{k}_{\omega}$ and $\boldsymbol{k}_{2\omega}$ represent the wave vectors corresponding to the fundamental and second-harmonic waves, respectively, while $\boldsymbol{G}_n$ denotes the n-order reciprocal lattice vector, as illustrated in Figure 3E, right. The reciprocal vector is defined as $\boldsymbol{G}_n = \frac{2\pi}{\Lambda}\hat{\boldsymbol{x}}$, where Λ is the period of the grating, and $\hat{\boldsymbol{x}}$ is the unit vector along the x axis. Based on the nonlinear Raman-Nath diffraction theory, the first-order diffraction angle θ of the generated second-harmonic wave is governed by the following relationship[48,49]:

$$\sin\theta = \frac{\boldsymbol{G}_n}{\boldsymbol{k}_{2\omega}} = \frac{n\lambda_{2\omega}}{\Lambda}, \qquad \text{(Equation 2)}$$

where $\lambda_{2\omega}$ denotes the wavelength of the second-harmonic wave. At an input fundamental wavelength of 800 nm, the experimentally determined angle θ of the first-order diffraction spot is approximately 1.2°, aligning closely with the theoretical prediction of 1.15°. The grating pattern and its nonlinear diffraction, achieved with the laser scanning direction perpendicular to the alignment direction, are provided in Figure 3F. Here, the periodically arranged laser-written domains are much slimmer compared to those written with the laser pencil along the alignment direction. In this configuration, the duty cycle of the grating is severely unbalanced, leading to more high-order diffraction orders compared to the result in Figure 3E. This demonstrates the critical influence of the laser scanning condition on the domain structure and diffraction behavior of the iced FNLC material. The ability to control and tailor such properties by adjusting the laser writing parameters opens up additional possibilities for designing and optimizing advanced diffractive devices for applications requiring complex nonlinear light manipulation.

To highlight the uniqueness of our direct-writing capability in the iced phase, we compared it with standard photoalignment techniques. In the high-temperature ferroelectric nematic phase (>120°C), photoalignment effectively patterns the LC. However, upon cooling to the room-temperature iced phase, the prepatterned grating structures degrade significantly due to polycrystalline grain growth (see Figure S19, resulting in strong light scattering and loss of diffraction efficiency. In contrast, our laser-written gratings (Figures 3E and 3F) are directly inscribed into the solid-like iced phase, yielding robust, stable periodic structures that are unattainable by cooling pre-aligned samples.

Building upon the successful demonstration of nonlinear beam steering with one-dimensional gratings, we further harnessed our femtosecond laser writing strategy to engineer a more sophisticated optical element: a forked grating (or vortex grating) of Λ = 15 μm within the iced ferroelectric nematic film. As illustrated in Figures 4A and 4B, this structure incorporates a designed topological defect (a dislocation with topological charge of m = 1) into the periodic domain lattice. The magnified view of Figure 4B is provided in Figure S20. When illuminated by the fundamental wave, this laser-written fork grating generates second-harmonic optical vortices carrying orbital angular momentum, as evidenced by the characteristic donut-shaped intensity profile of the diffracted beams (Figure 4C). It is worth noting that the central zero-order beam retains a Gaussian-like intensity profile (solid spot), while the diffracted orders carrying orbital angular momentum exhibit the characteristic doughnut shape. This observation aligns with the nonlinear diffraction theory and our simulations (Figure 4D), confirming the topological charge transfer. This result signifies that our direct-writing technique can imprint not only periodic nonlinear susceptibilities ($\chi^{(2)}$) but also a complex phase structure, including singularities, into the material.

DISCUSSION

To the best of our knowledge, this is the first demonstration of femtosecond laser writing of ferroelectric soft materials. Our strategy transforms the iced ferroelectric nematic—previously considered an "unpatternable" state—into a highly versatile

Please cite this article in press as: Chen et al., Thermoelectric-flow synergy for femtosecond laser writing of iced ferroelectric nematics, Matter (2026), https://doi.org/10.1016/j.matt.2026.102766

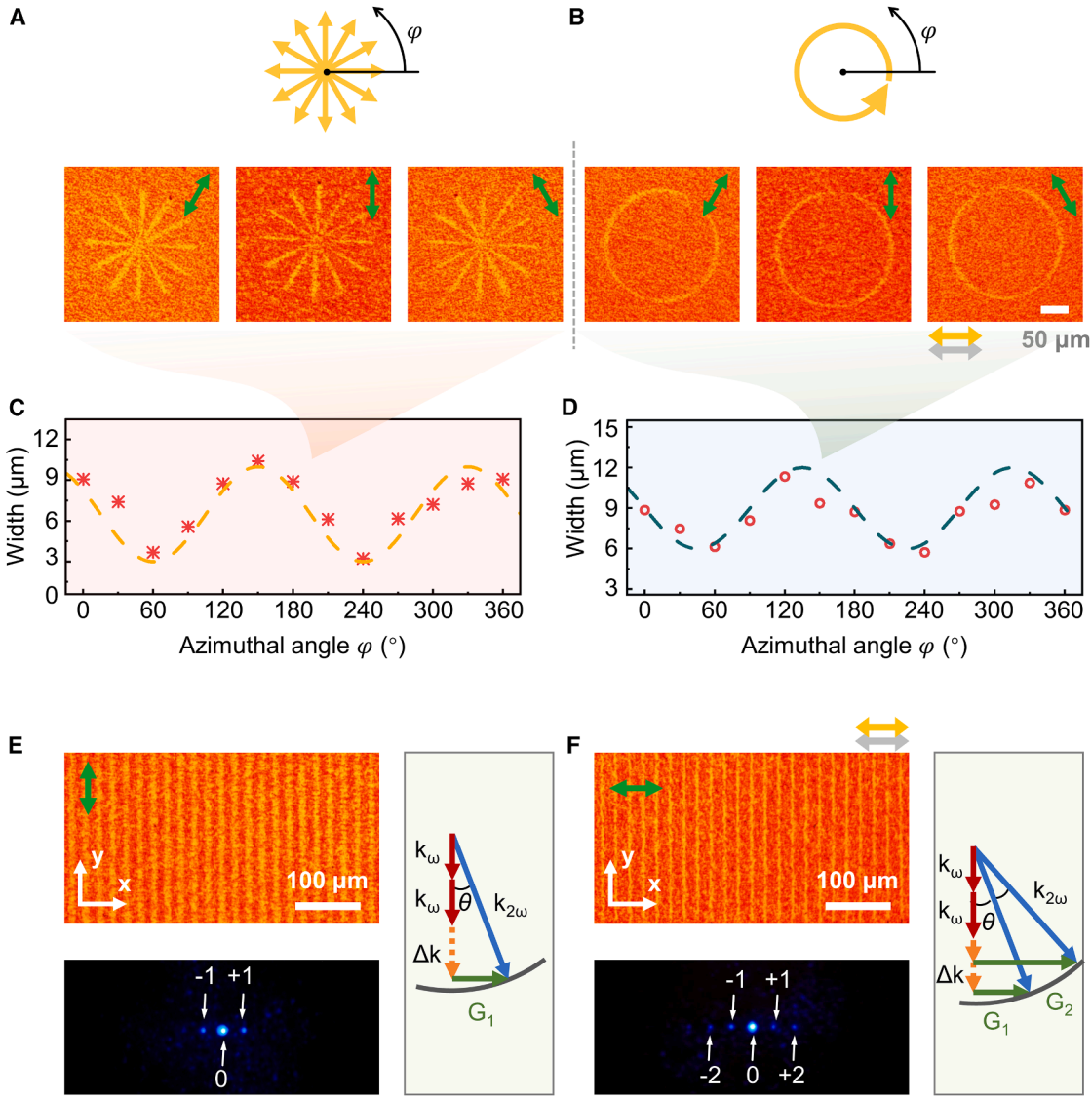

Figure 3. Designing iced FNLC domain structures for nonlinear optical modulation

(A and B) Radial and azimuthal domain patterning of the iced RM734 by femtosecond laser writing. The orange arrows show the direction of the laser writing. The green arrows show the rubbing alignment. The transmission axes of the polarizer and analyzer are indicated by gray and yellow arrows, respectively. The femtosecond laser energy is 450 mW. The scale bars are 50 μm.

(C and D) Relationships of the domain width and the azimuthal angle (φ) corresponding to the domain patterns in (A) and (B).

(E) POM texture of the nonlinear Raman-Nath grating with the laser writing direction parallel to the rubbing alignment, phase-matching configuration for nonlinear Raman-Nath diffraction, and the nonlinear diffraction pattern. The fabricated line domain width is 9.3 μm with a period of $\Lambda = 20$ μm. The scale bars are 100 μm. The pumping wavelength of the fundamental wave is 800 nm.

(F) POM texture of the nonlinear LC grating, phase-matching configuration for nonlinear Raman-Nath diffraction, and the diffraction pattern under the condition of laser scanning direction perpendicular to the rubbing alignment. The fabricated line domain width is 4.9 μm with a period of $\Lambda = 20$ μm. The transmission axes of the polarizer and analyzer are indicated by gray and yellow arrows, respectively.

platform for both fundamental research and applied photonics. The uniqueness of this platform lies in its thermoelectric-flow synergistic self-assembly mechanism, which operates independently of pre-existing surface alignment. By interacting with a system capable of undergoing local and transient phase transitions, the laser enables a synergistic interplay of thermal, fluid, and electric fields that dictates the final polar structure. This mechanism not only facilitates the creation of functional device architectures but also opens avenues for studying rich non-equilibrium phenomena in light-matter interactions, offering fundamental insights for reconfigurable nonlinear photonics and quantum optics. Specifically, the generation of a spherically radial thermoelectric field allows for all-optical, omnidirectional domain engineering, enabling the manipulation of local electric

Please cite this article in press as: Chen et al., Thermoelectric-flow synergy for femtosecond laser writing of iced ferroelectric nematics, Matter (2026), https://doi.org/10.1016/j.matt.2026.102766

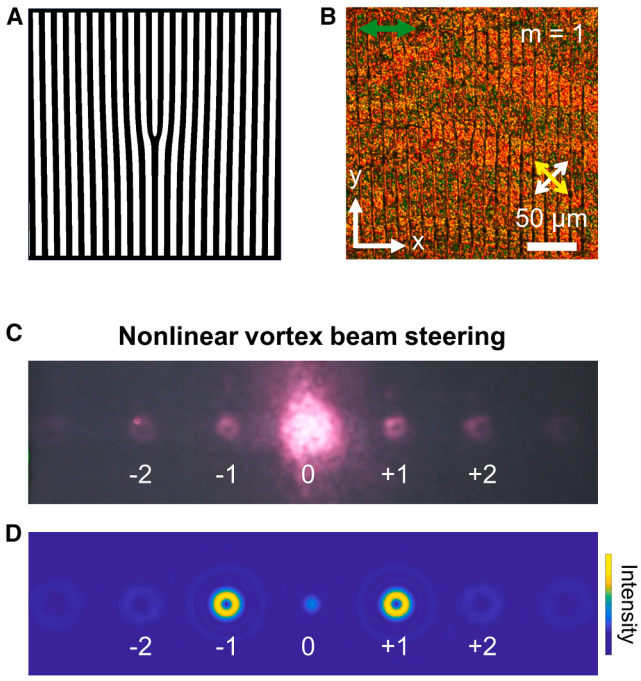

Figure 4. Laser-written nonlinear fork grating in rubbing-aligned iced RM734

(A) Laser scanning trajectory for the fabrication of the fork grating.

(B) POM image depicting the resultant nonlinear domain structure. Fork grating period Λ = 15 μm. Scale bars: 50 μm. Green arrows indicate the rubbing alignment direction. The transmission axes of the polarizer and analyzer are indicated by white and yellow arrows, respectively.

(C) Nonlinear beam steering of second-harmonic optical vortices. Fundamental wave: 800 nm. The apparent color shift of the diffraction pattern from its true spectral composition is due to long-exposure imaging.

(D) Simulated diffraction intensity distribution of a fork-shaped grating.

polarization at arbitrary orientations dictated by the laser scanning direction, which is unachievable in ferroelectric crystals. Crucially, we have confirmed that the RM734 material remains chemically stable under the employed laser writing conditions, with no signatures of photochemical degradation or crosslinking observed. Nonlinear wavefront shaping through direct laser writing of iced ferroelectric nematics is realized, marking a great advancement. Unlike conventional ferroelectric domain engineering methods that often rely on intricate lithography of electrode surfaces or complex multi-beam interference poling, our approach utilizes a single focused femtosecond laser beam to simultaneously induce a local phase transition and define the ferroelectric polarization pattern in a single step. This intrinsic "top-down" strategy offers unparalleled flexibility for generating arbitrary $\chi^{(2)}$ patterns, ranging from simple gratings to complex vortex generators, without the need for prefabricated masks or electrodes.

Looking forward, the potential of this femtosecond laser writing platform extends far beyond the current demonstration. It holds immense potential for emerging photonic applications. Given the unique properties of LCs[50–52]—such as tunable anisotropy and reconfigurability—this method may offer pathways for constructing practical functional microstructures. For instance, laser-induced patterning in initially disordered iced FNLC domains could have potential in forming complex skyrmionic structures,[53,54] potentially benefiting further photonic computing,[55] imaging,[56] and beyond.[57] Furthermore, the ability to locally modulate $\chi^{(2)}$ at the microscale is critical for programmable nonlinear holography and reconfigurable nonlinear optical diffractive elements.[58,59] This versatility underscores the transformative potential of our methodology, paving the way for reconfigurable soft photonic devices—from dynamically tunable meta-optics to programmable quantum light sources—and establishing a general platform for laser domain engineering in organic ferroelectric fluids. In addition, the inherent phase-change dynamics and excellent external-field reconfigurability of these laser-written devices further enhance their versatility for dynamic photonic systems. This approach paves the way for the application of ferroelectric nematics in a host of advanced technologies, including high-efficiency frequency mixing, ultrafast all-optical switching, quantum information processing via entangled photon generation, and high-density non-volatile ferroelectric memory.

METHODS

Materials

We synthesized RM734 following the procedures described in previous [11,30–32] to investigate its physical properties and written behaviors at room temperature. The agent SD1 (provided by Nanjing Ningcui Optical Technology Co., Ltd., China) was used for the photoalignment. SD1 molecules tend to align themselves perpendicular to the local linear polarization of light. SD1 molecules undergo isomerization upon absorbing ultraviolet photons and eventually align perpendicularly to the local polarization due to their dichroic absorption properties.[60,61] SD1 is rewritable, with only the final photo reorientation being recorded. Notably, once the LC material is infiltrated, the SD1 layer supplies sufficiently high anchoring energy to guide the arrangement of RM734 molecules in its liquid crystalline phases through intermolecular interactions.

Fabrications

Indium-tin-oxide (ITO)-coated glass substrates were first ultrasonically cleaned and then cleaned with UV ozone. For photoalignment cells, we use these substrates spin-coated with an SD1 photoalignment layer. The process is as follows. The alignment agent SD1 was dissolved in dimethylformamide at 0.35 wt %, spin-coated onto the substrates, and annealed at 100°C for 10 min. After that, two glass substrates were separated by spacers and assembled into a cell using a UV-curing adhesive. The thickness of the cell was measured using micro-interferometer. In order to achieve on-demand spatial orientations of SD1, empty cells were placed at the image plane of the digital micromirror device-based microlithography system to record the target patterns via a partly overlapping multistep exposure process with synchronous polarization control. After that, the RM734 material was infiltrated into LC cells at 188°C and slowly cooled to room temperature. If needed, an annealing process was carried out to drive the possible alignment of LC molecules on top of the SD1 layer. The uniform rubbing-aligned LC cells

were purchased from JCOPTIX China. If not specifically denoted, the tests in our work employed LC cells with a cell gap of ~10 μm. We also fabricated cells with no preset alignment (bare glass). An analysis of the optical anisotropy properties of the sample under a crossed-POM revealed that the laser-written domains exhibit nearly isotropic characteristics (Figure S21), consistent with those observed in uniformly photoaligned samples. This result further demonstrates the ineffectiveness of the preset alignment for iced FNLCs and confirms that the writing mechanism is intrinsic to the laser-material interaction, independent of a pre-aligned condition.

The laser writing process is as follows. A 10-μm-thick, uniformly aligned LC film is mounted on a nanopositioning stage capable of three-dimensional movements with a resolution of approximately 5 nm, as shown in Figure S4. The light source is a mode-locked Ti:sapphire laser (Chameleon Vision-S, Coherent), which generates 800 nm wavelength pulses with a 75-femtosecond duration and an 80 MHz repetition rate. The light power can be adjusted using a half-wave plate followed by a polarizer. The laser beam is linearly polarized and focused within the iced RM734 film using microscope objectives with numerical apertures NAs of 0.3 (10×). The polarization is parallel to the preset alignment direction. The calculation of the focused laser spot size is provided in Note S2. The nanopositioning stage moves the sample in the *x*-*y* plane, allowing the focused beam to scan across the sample. The fabrication process is monitored in real-time using a charge-coupled device. During the laser writing process, we carefully monitored the stability of the samples. The RM734 material used in this study is chemically stable under the femtosecond laser irradiation conditions employed (MHz repetition rate, selected power window). In addition, we disassembled the LC cells after writing at high power (500+ mW) and cleaned the substrates. Inspection of the ITO layer under an optical microscopy (without polarizers) revealed no significant damage to the conductive layer. This is likely because the central point of laser is focused within the bulk LC layer (thickness ~10 μm) not the ITO surface, as shown in Figure S22.

Characterizations

The textures of RM734 material were captured using a POM (DM2700P, Leica), which allows for detailed observations of the texture and optical anisotropic properties. The excitation fundamental waves for nonlinear beam steering were produced by a Ti:-sapphire femtosecond laser (Chameleon Vision S, Coherent) with a 75 femtosecond pulse duration, 80 MHz pulse repetition rate, operating at a central wavelength at 800 nm. The laser power was measured using a thermal power meter (S401C, Thorlabs). The phase transition behavior was characterized using a differential scanning calorimeter (Mettler Toledo DSC1, STARe).

RESOURCE AVAILABILITY

Lead contact

Requests for further information and resources should be directed to and will be fulfilled by the lead contact, Ling-Ling Ma (malingling@nju.edu.cn).

Materials availability

This study did not generate new unique reagents.

Data and code availability

Any additional information required to reanalyze the data reported in this paper is available from the lead contact upon request.

ACKNOWLEDGMENTS

This work was supported by the National Key Research and Development Program of China (no. 2022YFA1405000 to Y.-Q.L.), National Natural Science Foundation of China (nos. T2488302 to Y.-Q.L., 62375119 to L.-L.M., 92463304 to Y.Z., and 12404381 to X.-Y.X.), Natural Science Foundation of Jiangsu Province (nos. BK20243067 to Y.-Q.L., BK20250164 to L.-L.M., BK20232040 to L.-L.M., and BK20230768 to X.-Y.X.), Open Research Fund of State Key Laboratory of Quantum Functional Materials (no. QFM2025KF006 L.-L.M.), and Fundamental Research Funds for the Central Universities (no. 2025300215 to L.-L.M.).

AUTHOR CONTRIBUTIONS

L.-L.M., X.-Y.X., Y.-Q.L., Y.Z., and K.-Y.G. conceived the idea and designed the experiments. K.-Y.G., X.-Y.X., L.-L.M., J.-T.P., C.C., M.-X.X., B.-H.Z., Y.W., and L.H. performed the experiments, including preparation of samples, femtosecond laser writing, optical characterization, and analysis of material, structural, and optical properties. X.-Y.X., Z.-X.C., and L.-L.M. developed theoretical models for laser-induced thermoelectric field. L.-L.M., K.-Y.G., X.-Y.X., Y.Z., and Y.-Q.L. wrote the manuscript with input from all authors. K.-Y.G., X.-Y.X., L.-L.M., J.-T.P., C.C., Y.-Q.L., L.H., Y.Z., and C.-Z.X. discussed the results and proofread the manuscript. L.-L.M., Y.Z., and Y.-Q.L. supervised the project.

DECLARATION OF INTERESTS

L.-L.M. and Y.-Q.L. et al. filed a US Utility patent application on the preparation method and application for ferroelectric liquid crystal material grating at room temperature based on femtosecond laser direct writing.

SUPPLEMENTAL INFORMATION

Supplemental information can be found online at https://doi.org/10.1016/j.matt.2026.102766.

Received: November 17, 2025
Revised: January 28, 2026
Accepted: March 13, 2026

REFERENCES

1. Xu, X., Wang, T., Chen, P., Zhou, C., Ma, J., Wei, D., Wang, H., Niu, B., Fang, X., Wu, D., et al. (2022). Femtosecond laser writing of lithium niobate ferroelectric nanodomains. Nature *609*, 496–501. https://doi.org/10.1038/s41586-022-05042-z.
2. Kwaaitaal, M., Lourens, D.G., Davies, C.S., and Kirilyuk, A. (2024). Epsilon-near-zero regime enables permanent ultrafast all-optical reversal of ferroelectric polarization. Nat. Photonics *18*, 569–573. https://doi.org/10.1038/s41566-024-01420-3.
3. Zhang, Z., Deng, C., Fan, X., Li, M., Zhang, M., Wang, X., Chen, F., Shi, S., Zhou, Y., Deng, L., et al. (2024). 3D Directional Assembly of Liquid Crystal Molecules. Adv. Mater. *36*, 2401533. https://doi.org/10.1002/adma.202401533.
4. Zeng, H., Martella, D., Wasylczyk, P., Cerretti, G., Lavocat, J.C.G., Ho, C.H., Parmeggiani, C., and Wiersma, D.S. (2014). High-resolution 3D direct laser writing for liquid-crystalline elastomer microstructures. Adv. Mater. *26*, 2319–2322. https://doi.org/10.1002/adma.201305008.
5. Malinauskas, M., Žukauskas, A., Hasegawa, S., Hayasaki, Y., Mizeikis, V., Buividas, R., and Juodkazis, S. (2016). Ultrafast laser processing of

materials: from science to industry. Light Sci. Appl. *5*, e16133. https://doi.org/10.1038/lsa.2016.133.

6. Lu, J., Tian, J., Poumellec, B., Garcia-Caurel, E., Ossikovski, R., Zeng, X., and Lancry, M. (2023). Tailoring chiral optical properties by femtosecond laser direct writing in silica. Light Sci. Appl. *12*, 46. https://doi.org/10.1038/s41377-023-01080-y.
7. Jia, Y., Wang, S., and Chen, F. (2020). Femtosecond laser direct writing of flexibly configured waveguide geometries in optical crystals: fabrication and application. Opto-Electronic Adv. *3*, 190042. https://doi.org/10.29026/oea.2020.190042.
8. Zhao, M., Wen, J., Hu, Q., Wei, X., Zhong, Y.-W., Ruan, H., and Gu, M. (2024). A 3D nanoscale optical disk memory with petabit capacity. Nature *626*, 772–778. https://doi.org/10.1038/s41586-023-06980-y.
9. Wang, X., Cao, Q., Wang, R., Cao, X., and Liu, S. (2023). Domain growth driven by a femtosecond laser in lithium niobate crystal. Opt. Lett. *48*, 566–569. https://doi.org/10.1364/ol.469202.
10. Guo, Y., Coccia, G., Kavatamane, V.K., Giakoumaki, A.N., Vetlugin, A.N., Ramponi, R., Soci, C., Barclay, P.E., Hadden, J.P., Bennett, A.J., and Eaton, S.M. (2025). Enhanced Quantum Magnetometry with a Femtosecond Laser-Written Integrated Photonic Diamond Chip. Nano Lett. *25*, 8096–8102. https://doi.org/10.1021/acs.nanolett.5c00148.
11. Mandle, R.J., Cowling, S.J., and Goodby, J.W. (2017). A nematic to nematic transformation exhibited by a rod-like liquid crystal. Phys. Chem. Chem. Phys. *19*, 11429–11435. https://doi.org/10.1039/c7cp00456g.
12. Nishikawa, H., Shiroshita, K., Higuchi, H., Okumura, Y., Haseba, Y., Yamamoto, S.I., Sago, K., and Kikuchi, H. (2017). A Fluid Liquid-Crystal Material with Highly Polar Order. Adv. Mater. *29*, 1702354. https://doi.org/10.1002/adma.201702354.
13. Lucchetti, L. (2024). A new twist in ferroelectric liquids. Science *384*, 1067–1068. https://doi.org/10.1126/science.adp8824.
14. Karcz, J., Herman, J., Rychłowicz, N., Kula, P., Górecka, E., Szydlowska, J., Majewski, P.W., and Pociecha, D. (2024). Spontaneous chiral symmetry breaking in polar fluid–heliconical ferroelectric nematic phase. Science *384*, 1096–1099. https://doi.org/10.1126/science.adn6812.
15. Sultanov, V., Kavčič, A., Kokkinakis, E., Sebastián, N., Chekhova, M.V., and Humar, M. (2024). Tunable entangled photon-pair generation in a liquid crystal. Nature *631*, 294–299. https://doi.org/10.1038/s41586-024-07543-5.
16. Kumari, P., Basnet, B., Lavrentovich, M.O., and Lavrentovich, O.D. (2024). Chiral ground states of ferroelectric liquid crystals. Science *383*, 1364–1368. https://doi.org/10.1126/science.adl0834.
17. Chen, X., Korblova, E., Dong, D., Wei, X., Shao, R., Radzihovsky, L., Glaser, M.A., Maclennan, J.E., Bedrov, D., Walba, D.M., and Clark, N.A. (2020). First-principles experimental demonstration of ferroelectricity in a thermotropic nematic liquid crystal: Polar domains and striking electro-optics. Proc. Natl. Acad. Sci. USA *117*, 14021–14031. https://doi.org/10.1073/pnas.2002290117.
18. Li, J., Nishikawa, H., Kougo, J., Zhou, J., Dai, S., Tang, W., Zhao, X., Hisai, Y., Huang, M., and Aya, S. (2021). Development of ferroelectric nematic fluids with giant-epsilon dielectricity and nonlinear optical properties. Sci. Adv. *7*, eabf5047. https://doi.org/10.1126/sciadv.abf5047.
19. Zhang, G.-Y., Ma, L.-L., Lin, E., Wang, Z.-Y., Pan, J.-T., Yang, J., Deng, M., Wei, Y., Ye, Y., Wang, N., et al. (2025). Periodically-modulated unipolar and bipolar orders in nematic fluids towards miniaturized nonlinear vectorial optics. Nat. Commun. *16*, 9419. https://doi.org/10.1038/s41467-025-64463-2.
20. Yang, J., Zou, Y., Li, J., Huang, M., and Aya, S. (2024). Flexoelectricity-driven toroidal polar topology in liquid-matter helielectrics. Nat. Phys. *20*, 991–1000. https://doi.org/10.1038/s41567-024-02439-7.
21. Nakajima, K., Kamifuji, H., Nakase, M., Nishi, K., Kikuchi, H., and Ozaki, M. (2025). Sub-microsecond Birefringence Modulation of Blue Phase Polymer-Templated Ferroelectric Nematic Liquid Crystal Induced by Voltage Reversal. ACS Appl. Opt. Mater. *3*, 601–606. https://doi.org/10.1021/acsaom.4c00523.
22. Nishikawa, H., Okumura, Y., Kwaria, D., Nihonyanagi, A., and Araoka, F. (2025). Spontaneous Twist of Ferroelectric Smectic Blocks in Polar Fluids. Adv. Mater. *37*, 2501946. https://doi.org/10.1002/adma.202501946.
23. Medle Rupnik, P., Hanžel, E., Lovšin, M., Osterman, N., Gibb, C.J., Mandle, R.J., Sebastián, N., and Mertelj, A. (2025). Antiferroelectric Order in Nematic Liquids: Flexoelectricity Versus Electrostatics. Adv. Sci. *12*, 2414818. https://doi.org/10.1002/advs.202414818.
24. Caimi, F., Nava, G., Fuschetto, S., Lucchetti, L., Paiè, P., Osellame, R., Chen, X., Clark, N.A., Glaser, M.A., and Bellini, T. (2023). Fluid superscreening and polarization following in confined ferroelectric nematics. Nat. Phys. *19*, 1658–1666. https://doi.org/10.1038/s41567-023-02150-z.
25. Pan, J.-T., Zhu, B.-H., Ma, L.-L., Chen, W., Zhang, G.-Y., Tang, J., Liu, Y., Wei, Y., Zhang, C., Zhu, Z.-H., et al. (2024). Nonlinear geometric phase coded ferroelectric nematic fluids for nonlinear soft-matter photonics. Nat. Commun. *15*, 8732. https://doi.org/10.1038/s41467-024-53040-8.
26. Mirri, G., Škarabot, M., and Muševič, I. (2015). In situ laser-imprinted surface realignment of a nematic liquid crystal. Soft Matter *11*, 3347–3353. https://doi.org/10.1039/c5sm00282f.
27. Jagodič, U., Vellaichamy, M., Škarabot, M., and Muševič, I. (2023). Surface alignment of nematic liquid crystals by direct laser writing of photopolymer alignment layers. Liq. Cryst. *50*, 1999–2009. https://doi.org/10.1080/02678292.2023.2242297.
28. del Pozo, M., Delaney, C., Bastiaansen, C.W.M., Diamond, D., Schenning, A.P.H.J., and Florea, L. (2020). Direct Laser Writing of Four-Dimensional Structural Color Microactuators Using a Photonic Photoresist. ACS Nano *14*, 9832–9839. https://doi.org/10.1021/acsnano.0c02481.
29. Xu, A., Nourshargh, C., Salter, P.S., He, C., Elston, S.J., Booth, M.J., and Morris, S.M. (2023). Laser-Written Tunable Liquid Crystal Aberration Correctors. ACS Photonics *10*, 3401–3408. https://doi.org/10.1021/acsphotonics.3c00907.
30. Mandle, R.J., Cowling, S.J., and Goodby, J.W. (2017). Rational Design of Rod-Like Liquid Crystals Exhibiting Two Nematic Phases. Chem.-Eur. J. *23*, 14554–14562. https://doi.org/10.1002/chem.201702742.
31. Mertelj, A., Cmok, L., Sebastián, N., Mandle, R.J., Parker, R.R., Whitwood, A.C., Goodby, J.W., and Čopič, M. (2018). Splay Nematic Phase. Phys. Rev. X *8*, 041025. https://doi.org/10.1103/PhysRevX.8.041025.
32. Sebastián, N., Cmok, L., Mandle, R.J., de la Fuente, M.R., Drevenšek Olenik, I., Čopič, M., and Mertelj, A. (2020). Ferroelectric-Ferroelastic Phase Transition in a Nematic Liquid Crystal. Phys. Rev. Lett. *124*, 037801. https://doi.org/10.1103/PhysRevLett.124.037801.
33. Boyd, R.W. (2020). Nonlinear Optics, 4th edn (Academic Press).
34. Xu, X.-Y., Huang, X.-L., Li, Z.-M., Gao, J., Jiao, Z.-Q., Wang, Y., Ren, R.-J., Zhang, H.P., and Jin, X.-M. (2020). A scalable photonic computer solving the subset sum problem. Sci. Adv. *6*, eaay5853. https://doi.org/10.1126/sciadv.aay5853.
35. Kawata, S., Sun, H.-B., Tanaka, T., and Takada, K. (2001). Finer features for functional microdevices. Nature *412*, 697–698. https://doi.org/10.1038/35089130.
36. Ródenas, A., Gu, M., Corrielli, G., Paiè, P., John, S., Kar, A.K., and Osellame, R. (2018). Three-dimensional femtosecond laser nanolithography of crystals. Nat. Photonics *13*, 105–109. https://doi.org/10.1038/s41566-018-0327-9.
37. Sun, K., Tan, D., Fang, X., Xia, X., Lin, D., Song, J., Lin, Y., Liu, Z., Gu, M., Yue, Y., and Qiu, J. (2022). Three-dimensional direct lithography of stable perovskite nanocrystals in glass. Science *375*, 307–310. https://doi.org/10.1126/science.abj2691.
38. Tadashi Akahane, T.A., Hideki Kaneko, H.K., and Munehiro Kimura, M.K. (1996). Novel Method of Measuring Surface Torsional Anchoring Strength of Nematic Liquid Crystals. Jpn. J. Appl. Phys. *35*, 4434. https://doi.org/10.1143/jjap.35.4434.

39. Padmini, H.N., Rajabi, M., Shiyanovskii, S.V., and Lavrentovich, O.D. (2021). Azimuthal Anchoring Strength in Photopatterned Alignment of a Nematic. Crystals *11*, 675. https://doi.org/10.3390/cryst11060675.

40. Lancry, M., Groothoff, N., Poumellec, B., Guizard, S., Fedorov, N., and Canning, J. (2011). Time-resolved plasma measurements in Ge-doped silica exposed to infrared femtosecond laser. Phys. Rev. B *84*, 245103. https://doi.org/10.1103/PhysRevB.84.245103.

41. Graziano, D.J., and Mackley, M.R. (1984). Disclinations observed during the shear of MBBA. Mol. Cryst. Liq. Cryst. *106*, 103–119. https://doi.org/10.1080/00268948408080182.

42. Alderman, N.J., and Mackley, M.R. (1985). Optical textures observed during the shearing of thermotropic liquid-crystal polymers. Faraday Discuss. Chem. Soc. *79*, 149–160. https://doi.org/10.1039/DC9857900149.

43. Rey, A.D. (1993). Analysis of shear flow effects on liquid crystalline textures. Mol. Cryst. Liq. Cryst. Sci. Technol., Sect. A *225*, 313–335. https://doi.org/10.1080/10587259308036237.

44. Bahr, C. (2025). Flow-induced disclination lines in nematic liquid crystals. Phys. Rev. E *112*, 045408. https://doi.org/10.1103/4lpd-x8b7.

45. Caimi, F., Nava, G., Barboza, R., Clark, N.A., Korblova, E., Walba, D.M., Bellini, T., and Lucchetti, L. (2021). Surface alignment of ferroelectric nematic liquid crystals. Soft Matter *17*, 8130–8139. https://doi.org/10.1039/d1sm00734c.

46. Liu, Y., Zhou, L., Wen, Y., Shen, Y., Sun, J., and Zhou, J. (2022). Optical Vector Vortex Generation by Spherulites with Cylindrical Anisotropy. Nano Lett. *22*, 2444–2449. https://doi.org/10.1021/acs.nanolett.2c00171.

47. Saltiel, S.M., Neshev, D.N., Krolikowski, W., Arie, A., Bang, O., and Kivshar, Y.S. (2009). Multiorder nonlinear diffraction in frequency doubling processes. Opt. Lett. *34*, 848–850. https://doi.org/10.1364/ol.34.000848.

48. Chen, Y., Ni, R., Wu, Y., Du, L., Hu, X., Wei, D., Zhang, Y., and Zhu, S. (2020). Phase-Matching Controlled Orbital Angular Momentum Conversion in Periodically Poled Crystals. Phys. Rev. Lett. *125*, 143901. https://doi.org/10.1103/PhysRevLett.125.143901.

49. Saltiel, S.M., Neshev, D.N., Krolikowski, W., Voloch-Bloch, N., Arie, A., Bang, O., and Kivshar, Y.S. (2010). Nonlinear Diffraction from a Virtual Beam. Phys. Rev. Lett. *104*, 083902. https://doi.org/10.1103/PhysRevLett.104.083902.

50. Yuan, C.-l., Chen, J.-j., Liu, B.-h., Sun, P.-z., Hu, H.-l., Tang, Y., Wang, Y.-f., Zhan, Y., Li, M., Zheng, Z.-g., and Li, Q. (2023). Hyper-stable field-stimulated soft cholesteric heliconical architectures. Matter *6*, 3555–3573. https://doi.org/10.1016/j.matt.2023.07.027.

51. Chen, H.-F., Tao, X.-Y., Zhu, B.-H., Pan, J.-T., Ma, L.-L., Chen, C., Zhu, W.-G., Chen, W., and Lu, Y.-Q. (2025). Reconfigurable nonlinear Pancharatnam-Berry diffractive optics with photopatterned ferroelectric nematics. Light Sci. Appl. *14*, 314. https://doi.org/10.1038/s41377-025-01981-0.

52. Wang, Z.-Y., Zhou, Z., Zhang, H., Wei, Y., Yu, H.-G., Hu, W., Chen, W., Dai, H.-T., Ma, L.-L., Qiu, C.-W., and Lu, Y.-Q. (2024). Vectorial liquid-crystal holography. eLight *4*, 5. https://doi.org/10.1186/s43593-024-00061-x.

53. He, C., Chen, B., Song, Z., Zhao, Z., Ma, Y., He, H., Luo, L., Marozsak, T., Wang, A.A., Xu, R., et al. (2025). A reconfigurable arbitrary retarder array as complex structured matter. Nat. Commun. *16*, 4902. https://doi.org/10.1038/s41467-025-59846-4.

54. Wang, A.A., Zhao, Z., Ma, Y., Cai, Y., Zhang, R., Shang, X., Zhang, Y., Qin, J., Pong, Z.-K., Marozsák, T., et al. (2024). Topological protection of optical skyrmions through complex media. Light Sci. Appl. *13*, 314. https://doi.org/10.1038/s41377-024-01659-z.

55. Wang, A.A., Ma, Y., Zhang, Y., Zhao, Z., Cai, Y., Qiu, X., Dong, B., and He, C. (2025). Perturbation-resilient integer arithmetic using optical skyrmions. Nat. Photonics *19*, 1367–1375. https://doi.org/10.1038/s41566-025-01779-x.

56. Ma, Y., Zhao, Z., Shen, Y., Chen, B., Wang, A.A., Cai, Y., Qin, J., Zhang, R., Zhang, Y., Cui, J., et al. (2025). Using optical skyrmions to assess vectorial adaptive optics capabilities in the presence of complex aberrations. Sci. Adv. *11*, eadv7904. https://doi.org/10.1126/sciadv.adv7904.

57. Qiu, X., Zhang, R., Ma, Y., Zhao, Z., Song, Z., Orr, A.C.J., Li, M., Kamal, W., Guo, J., Castrejón-pita, A.A., et al. (2025). Complex Structured Light Generation Using Printed Liquid Crystal Droplets. Adv. Opt. Mater. *13*, e02276. https://doi.org/10.1002/adom.202502276.

58. Ren, M., Xu, J., Lan, P., Lu, P., Li, Z.-Y., Hong, L.-H., Wang, Y., Bai, Z., Lv, Z., Zhou, Z.-Y., et al. (2023). Roadmap on nonlinear optics–focus on Chinese research. J. Phys. Photonics *5*, 032501. https://doi.org/10.1088/2515-7647/acdb17.

59. Mao, N., Zhang, G., Tang, Y., Li, Y., Hu, Z., Zhang, X., Li, K., Cheah, K., and Li, G. (2022). Nonlinear vectorial holography with quad-atom metasurfaces. Proc. Natl. Acad. Sci. USA *119*, e2204418119. https://doi.org/10.1073/pnas.2204418119.

60. Chigrinov, V., Pikin, S., Verevochnikov, A., Kozenkov, V., Khazimullin, M., Ho, J., Huang, D.D., and Kwok, H.-S. (2004). Diffusion model of photoaligning in azo-dye layers. Phys. Rev. E *69*, 061713. https://doi.org/10.1103/PhysRevE.69.061713.

61. Wu, H., Hu, W., Hu, H.C., Lin, X.W., Zhu, G., Choi, J.W., Chigrinov, V., and Lu, Y.Q. (2012). Arbitrary photo-patterning in liquid crystal alignments using DMD based lithography system. Opt. Express *20*, 16684–16689. https://doi.org/10.1364/OE.20.016684.